Front. Optoelectron. 2014, 7(3): 277–292
DOI 10.1007/s12200-014-0424-4

REVIEW ARTICLE

Recent developments in graphene-based optical modulators

Ran HAO (✉), Jiamin JIN, Xinchang WEI, Xiaofeng JIN, Xianmin ZHANG, Erping LI (✉)

Department of Information Science and Electronics Engineering, Zhejiang University, Hangzhou 310027, China

Abstract Graphene has shown promising perspectives in optical active components due to the large active-control of its permittivity-variation. This paper systematically reviews the recent developments of graphene-based optical modulators, including material property, different integration schemes, single-layer graphene-based modulator, multi-layer and few-layer graphene-based modulators, corresponding figure-of-merits, wavelength/temperature tolerance, and graphene-based fiber-optic modulator. The different treatments for graphene's isotropic and anisotropic property were also discussed. The results showed graphene is an excellent material for enhancing silicon's weak modulation capability after it is integrated into the silicon platform, and has great potentials for complementary metal oxide semiconductor (CMOS) compatible optical devices, showing significant influence on optical interconnects in future integrated optoelectronic circuits.

Keywords dynamic control, effective mode index (n_{eff}), electro-absorption (EA) effect, electro-refraction (ER) effect, graphene, Mach-Zehnder interferometer (MZI), optical modulators

1 Introduction

Silicon photonic interconnection is a promising technology for intra-/interchip data link due to its unique combination of low fabrication cost, performance enhancement from integration, and compatibility with the world's most widely used technology in electronics, complementary metal oxide semiconductor (CMOS) [1,2]. The interconnections based on silicon photonics, including guiding, modulation, detection, assembly, etc, are the leading candidates to achieve future optical integrated circuits. As one of the main functionalities for optical interconnection, silicon-based optical modulator has attracted large amount of attentions. Optical modulator is a device that is used to modulate (alter) the characteristics of a light beam, categorized as amplitude, phase or polarization modulators. In addition, electro-optical modulators can be also classified as either electro-refractive or electro-absorptive one. By applying an electric field to the material, the real and imaginary part of the refractive index can be changed. A change in the real part of the refractive index caused by the applied voltage is known as the electro-refraction (ER) effect, whereas a change in the imaginary part of the refractive index is known as the electro-absorption (EA) effect. The electric effects that traditionally cause either ER or EA are Pockels effect, Kerr effect, Franz–Keldysh effect and plasma dispersion effect [3]. However, these effects are too weak in pure silicon material at the communication wavelengths so that it usually needs an extremely large arm length which results in large footprint as well as highdrive voltage to reach the required modulation, e. g., recent result has showed Mach-Zehnder Interferometer (MZI) optical modulator has the length of 4 mm [4]. In addition, the side-effect introduced to the pass-band and stability after applying some enhancement methods is still challenging. Even with the doping of silicon, the modulation speed is limited due to the low carrier mobility in silicon, e.g., the best reported modulation speed is up to 50 Gbit/s and difficult to be further improved [5–8]. To overcome these fundamental bottlenecks, novel materials need to be explored so that they can provide better modulation capability and CMOS compatibility simultaneously.

Graphene, the two-dimensional (2D) carbon sheet in honeycomb lattice with only one-atom-layer thickness, has attracted lots of interest due to its remarkable mechanical, electric, magnetic thermal and optical properties. It has the merits of small effective electron mass, transparent to visible light, giant nonlinear coefficient [9,10], etc. Graphene provides the highest carrier mobility that is much larger than that of silicon, and much stronger interaction with light for the electro-refractive or electro-absorptive effects in a broad frequency regime [3,11–13], which make it an excellent material for the high performance optical modulator. Additionally, the conductivity of graphene can be modified by means of chemical

Received March 3, 2014; accepted April 26, 2014

E-mail: rhao@zju.edu.cn, liep@zju.edu.cn

doping, electric field, or magnetic fields [14,15]. When the imaginary part of graphene conductivity is negative, graphene supports the transverse magnetic mode noted as surface plasmon polaritons (SPP) [14–19], displaying potentials for highly tunable SPP modulator applications [20–23]. This is why a large amount of research attention has been focused on the graphene-based optical modulator.

In this paper, we systematically reviewed the mechanism and recent developments for various graphene-based optical modulators. The following of this manuscript is arranged as follow: Section 2 presented the optical material properties of a freestanding monolayer graphene. In Section 3, the performances of monolayer graphene-based modulators were reviewed, including the EA modulator and the ER modulator. And the difference between isotropic and anisotropic graphenes is compared. In Section 4, we reviewed recent studies on the multi-layer and the few-layer graphene-based modulators, and the tolerances for temperature and wavelength variation were discussed. In Section 5, we reviewed recent studies on graphene-based fiber modulators. In Section 6, the conclusion was made.

2 Optical material properties of single-layer graphene

In the mid-infrared wavelengths, when graphene is doped with a certain concentration of electron or hole, it is demonstrated both theoretically [14,24–27] and experimentally [28–30] that graphene surface plasmons (GSP) can propagate through the graphene sheet. Graphene is an excellent platform for plasmonic devices owing to its large active-control of its conductivity-function that is not seen in noble metals [14]. The conductivity of graphene can be modified by means of chemical doping, electric field, or magnetic fields according to the Kubo formula [31]:

$$\begin{aligned}\delta(\omega,\mu_c,\Gamma,T) =&\sigma_{\text{intra}}(\omega,\mu_c,\Gamma,T)+\sigma_{\text{inter}}(\omega,\mu_c,\Gamma,T)\\ =&\frac{-ie^2}{\pi\hbar^2(\omega+i2\Gamma)}\left[\int_0^\infty \varepsilon\left(\frac{\partial f_d(\varepsilon)}{\partial\varepsilon}-\frac{\partial f_d(-\varepsilon)}{\partial\varepsilon}\right)d\varepsilon\right]\\ &-\frac{ie^2(\omega+i2\Gamma)}{\pi\hbar^2}\left[\int_0^\infty \frac{f_d(-\varepsilon)-f_d(\varepsilon)}{(\omega+i2\Gamma)^2-4(\varepsilon/\hbar)^2}d\varepsilon\right],\end{aligned} \tag{1}$$

where Γ represents the scattering rate, μ_c represents the chemical potential, $f_d(\varepsilon)$ is the Fermi-Dirac distribution, i is the imaginary unit, e is the charge of the electron, $\hbar$ is the reduced Planck's constant, ω is the radian frequency, and T is the temperature.

The chemical potential of graphene depends on the carrier density which can be controlled by the external gate voltage, electric field, magnetic field, and chemical doping. The imaginary part of graphene conductivity can attain negative and positive values in different ranges of frequencies depending on the level of chemical potential. The complex conductivity of a free-standing isolated graphene — computed from the Kubo formula, which is in agreement with experimental results [31] — shows regions of frequencies and chemical potentials for which σ_g, $i<0$, whereas for other regions σ_g, $i>0$. When σ_g, $i<0$, the graphene sheet acts like a thin metallic layer, therefore it is possible to transfer surface plasmon called GSP.

Since graphene is a 2D material, we could not directly derive its permittivity from the above conductivity. Instead, a special technique to model the 3D graphene permittivity is applied, which was first introduced by Vakil and Engheta [14]. By defining a certain thickness Δ of graphene, (e.g., here we take Δ = 0.7 nm in accordance with Refs. [3,20,32]), the "pseudo" bulk-conductivity can be defined as σ_ω/Δ, and thus the "pseudo" permittivity can also be defined as $\varepsilon(\omega) = 1 + i\sigma(\omega)/(\varepsilon_0\omega\Delta)$. The obtained permittivity values were used strictly in conjunction with the defined thickness value.

Figure 1 shows the permittivity and conductivity of an infinite graphene sheet at the wavelength λ = 1550 nm. It can be seen that there is a dip in the curve of permittivity magnitude, and the epsilon-near-zero (ENZ) point is obtained at the chemical potential μ_{c0}= 0.513 eV where the absolute value of epsilon is approaching zero. When the chemical potential $\mu_c<\mu_{c0}$, both the real and imaginary part of the permittivity (Re($\varepsilon_{//}$) and Im($\varepsilon_{//}$)) have the positive sign so that the graphene layer behaves like a dielectric material. When the chemical potential is gradually increased, the "dielectric graphene" is gradually transforming into "metallic graphene" at the transition chemical potential μ_{c0}= 0.513 eV. There exists a range where in which both Re($\varepsilon_{//}$) and Im($\varepsilon_{//}$) are very close to zero called ENZ point. When $\mu_c>0.52$ eV, Re($\varepsilon_{//}$) becomes negative and Im($\varepsilon_{//}$) is approaching zero which means the graphene layer acts like a metallic layer, and the graphene layer is then fabulous to transfer surface plasmon polaritons (SPP) [11], displaying much more potential for future optoelectronic devices. Compared with traditional metal plasmonic devices, graphene plasmonic devices are very compact due to the highly-compressed GSP wavelength (strong subwavelength confinement) [14,33], and demonstrate active waveguide-based switching [3,12] as well as low losses [15], which could lead to an exciting new area of research in mid-infrared graphene plasmonic nanocircuits.

Especially, the gate-voltage dependent feature [14] that the chemical potential of graphene can be controlled in real-time by external gate voltages, which has been confirmed in experiment [28–30], is opening up an opportunity for electrically controlled plasmonic devices. Therefore, it is possible to tailor the SPP waves by varying

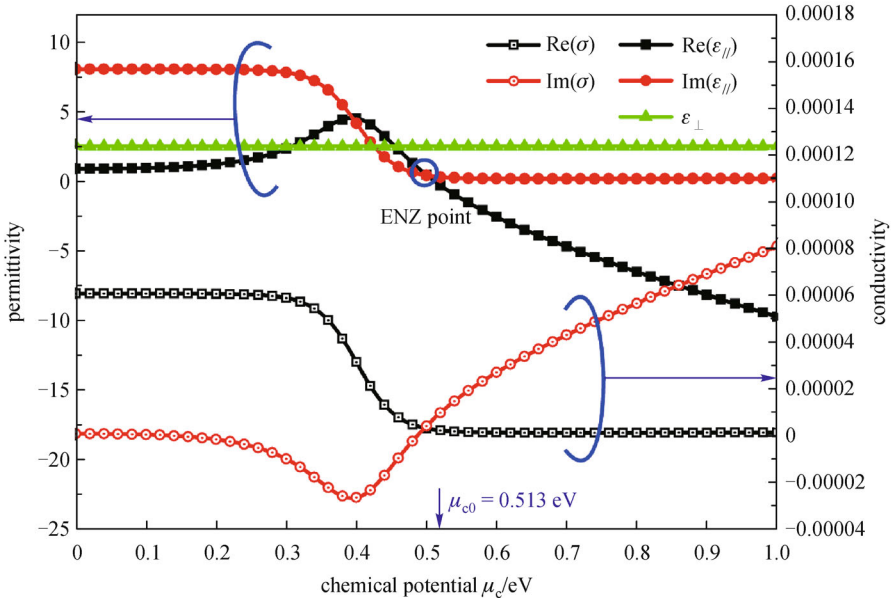

Fig. 1 Conductivity and permittivity of an infinite graphene sheet (the wavelength is fixed at 1550 nm) (reprinted from Ref. [20])

the chemical potential of graphene without re-optimizing and re-fabricating the nano-structures. The corresponding waveguides constructed on a single flake of graphene [14] by non-uniform conductivity patterns, optical spatial switches [34], splitters [35], and directional couplers [36], have been reported in detail and exhibit obvious advantages over the noble metals.

3 Single-layer graphene-based modulator

In the first place, it is important to clarify how graphene is integrated into the silicon waveguide. So far, there have been two kinds of approaches. One relies on the structure that graphene is placed on the top surface of the silicon waveguide and the thickness of silicon waveguide is optimized. For example, a graphene-based modulator at frequencies over 1 GHz and a broad operation bandwidth from 1.35 to 1.6 μm was proposed [3]. The modulator has the advantage of CMOS compatible, broadband and ultra-small footprint (25 μm^2) [3]. The other approach tries to embed graphene in the center of silicon waveguide so that graphene is overlapped with the maximum field, e.g., an electric-absorption modulator was demonstrated with extremely short length of 800 nm and modulation depth of 3 dB [24] based on such geometry. Yang et al. designed a low-chirp graphene-embedded Mach-Zehnder (MZ) modulator with the arm length of 43.54 μm and extinction ratio of 34.7 dB [37]. Compared with previous approach, the second one has shown better graphene-light interaction because of the good match between graphene and the maximum field in silicon waveguide. In order to maximize graphene's influence, we consider the second approach throughout this manuscript.

The effective modal refractive index (n_{eff}) of the graphene-embedded silicon waveguide (GESW, as depicted in Fig. 2(a)) is the critical parameter that determines the overall GESW properties. The real part of the index (Re(n_{eff})) is linear to mode's phase information via: $\varphi = k_0 \text{Re}(n_{\text{eff}})L$, where k_0 is the wave number in vacuum and L is the propagation distance. The imaginary part of the index (Im(n_{eff})) is related to the propagation loss α through $\alpha = 8.68 k_0 \text{Im}(n_{\text{eff}})$ [20]. Therefore, the configuration of an optical modulator can be implement by changing either the Re(n_{eff}) or Im(n_{eff}): the former one is typically the phase modulator, while the later one is the amplitude modulator. The calculated Re(n_{eff}) and the Im(n_{eff}) for the proposed GESW under the chemical potential from 0 to 1 eV is shown as Fig. 2(b). According to the modal theory, the n_{eff} is then calculated from

$$n_{\text{eff}} = \frac{\zeta}{k_0} = \frac{\beta}{k_0} + i\frac{\delta_z}{k_0}, \tag{2}$$

where ζ is the eigenvalue of the system, β is the propagation constant, and δ_z is the attenuation constant. In Fig. 2(b), the n_{eff} of the proposed waveguide is lower than silicon's refractive index (3.45) at all chemical potentials. An inflection point is observed in the Re(n_{eff}) curve at μ_c = 0.4 eV, where n_{eff} changes intensively near the inflection point. If comparing Fig. 2(b) with Fig. 1, a similarity between the n_{eff} curve and graphene's $\varepsilon_{//}$ curve can be found. It is thus inferred that n_{eff} is proportional with $\varepsilon_{//}$, and one could control n_{eff} to the desired value in terms of simply changing n_{eff}.

According to the electromagnetic theory, the permittivity of the overall mode can be defined through [20]

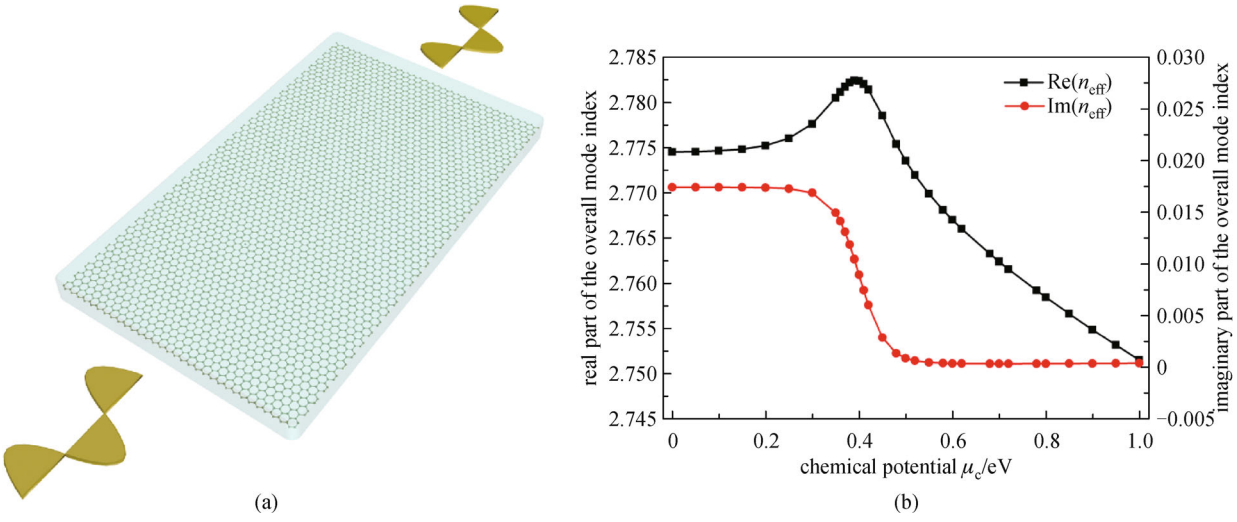

Fig. 2 (a) 3D view of GESW; (b) real and imaginary parts of effective modal index variation under different chemical potentials for GESW (reprinted from Ref. [20])

$$\varepsilon_{\text{eff}} = \frac{D_{\text{eff}}}{E_{\text{eff}}} = \frac{\dfrac{\varepsilon_{\text{si}} \oiint E_{\text{si}} \mathrm{d}S_{\text{si}} + \varepsilon_{\text{air}} \oiint E_{\text{air}} \mathrm{d}S_{\text{air}} + \varepsilon_{//} \oiint E_{\text{g}} \mathrm{d}S_{\text{g}}}{\mathrm{d}S}}{\dfrac{\oiint E_{\text{si}} \mathrm{d}S_{\text{si}} + \oiint E_{\text{air}} \mathrm{d}S_{\text{air}} + \oiint E_{\text{g}} \mathrm{d}S_{\text{g}}}{\mathrm{d}S}} = \frac{\varepsilon_{\text{si}} En_{\text{si}} + \varepsilon_{\text{air}} En_{\text{air}} + \varepsilon_{//} En_{\text{g}}}{En}, \tag{3}$$

where ε_{si} and ε_{air} are the permittivity of silicon and air respectively, and $\varepsilon_{//}$ is the in-plane permittivity of graphene; En_{si}, En_{air} and En_{g} are the electric field intensity inside the silicon, air and graphene regions separately; En_{si}, En_{air}, En_{g} are the corresponding energy inside the silicon, air and graphene region; S_{si}, S_{air}, and S_{g} are the area for silicon, air, graphene region, respectively, S is the area for the sum of all regions. Due to ε_{si}, ε_{air} are constant, the n_{eff} of the overall mode can be derived from

$$n_{\text{eff}} = \sqrt{\frac{D_{\text{eff}}}{E_{\text{eff}}}} = \sqrt{\frac{12En_{\text{si}} + En_{\text{air}}}{En} + \varepsilon_{//}\frac{En_g}{En}} \approx \sqrt{\frac{12En_{\text{si}} + En_{\text{air}}}{En}} \times \left[1 + \frac{1}{2}\frac{En}{12En_{\text{si}} + En_{\text{air}}}\varepsilon_{//}\right]. \tag{4}$$

Because the graphene sheet has limited thickness and the electric field must be continuous along the graphene-silicon interface, the energy ratios En_{si}/E_n, En_{air}/E_n, En_{g}/E_n vary slightly under different chemical potentials. According to the eigenmode analysis results, these ratios are almost constant under all chemical potentials. Therefore, there is only one parameter $\varepsilon_{//}$ is uncertain in Eq. (5), the relationship between n_{eff} and $\varepsilon_{//}$ is thus obtained in the form of a linear relationship after expanding Eq. (5) in terms of Taylor series. Figure 3 shows the relationship between n_{eff} and graphene's $\varepsilon_{//}$ in two different approaches. The black lines represent the analytical results from the eigen-mode solver of the finite element method, the red dot lines are the numerical results from Eq. (5). In Fig. 3, there is only a tiny difference of the slopes between the black line and the red dot line. The accordance between the analytical results and numerical results has confirmed the correction of our inference: the overall mode index n_{eff} is proportional to graphene's in-plane permittivity $\varepsilon_{//}$. Because the modal effective index (regarded as the key parameter for a waveguide) is simply linked to only one of its permittivity parameter in the proposed GESW, it opens great opportunities to control the waveguide's performances in a more flexible way. The linear relationship can also explain why the waveguide has low loss when $\mu_c > \mu_{c0}$. Furthermore, compared with the silicon waveguide where the maximum index variation is at the level of 10^{-4} for the doped silicon, the proposed GESW can have a variation of n_{eff} up to 0.035 (as shown in Fig. 2), which is several orders of magnitude larger than silicon's best capability.

3.1 Graphene-based electric-refractive modulator

The impressive large value of Δn_{eff} is great appreciated for the modulator designs based on ER effect, such as MZ modulator, as shown in the schematic picture of Fig. 4(a). Let us first fix one chemical potential at $\mu_{c1} = 1$ eV because it is the smallest Im(n_{eff}), then sweep the other chemical potential μ_{c2} from 0.39 to 0.95 eV according to the linear portion of the black curve in Fig. 2. With μ_{c2} changing, the

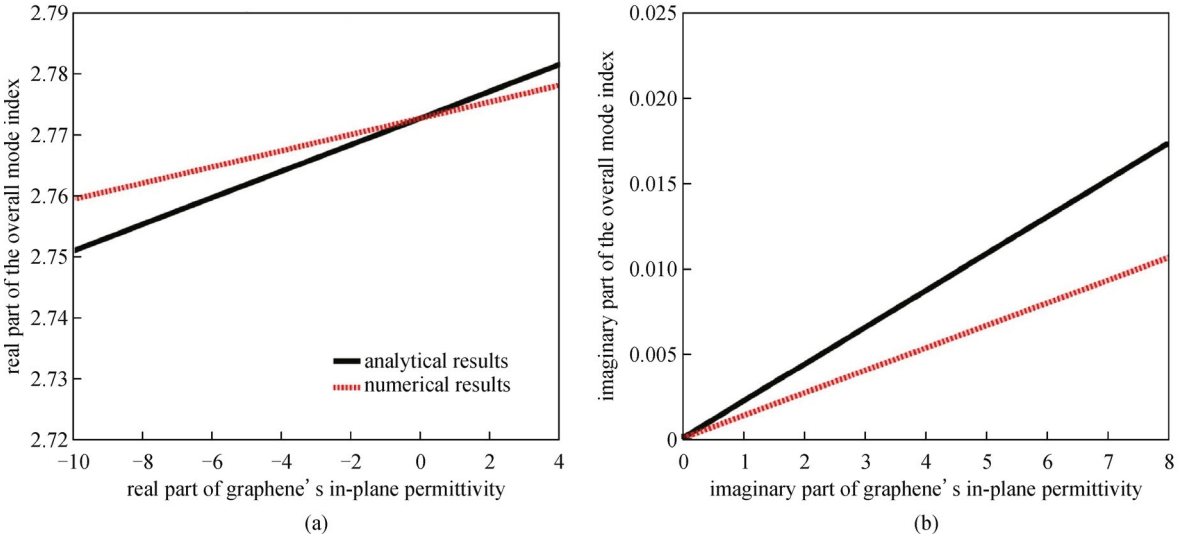

Fig. 3 (a) Linear relationship between the real part of effective modal index and the real part of graphene's in-plane permittivity; (b) linear relationship between the imaginary part of effective modal index and the imaginary part of graphene's in-plane permittivity (reprinted from Ref. [20])

corresponding Δn_{eff} will be modified, thus the required arm length L_π to reach the π phase shift is modified. L_π can be calculated through $\pi = L_\pi \times \Delta n_{\text{eff}}$. Figure 4(b) has shown the relationship between L_π and $\Delta\mu_c$ while μ_{c1} is fixed at 1 eV. The general trend is that L_π becomes smaller with the increase of $\Delta\mu_c$, but after $\Delta\mu_c$ is increased to 0.3 eV, the decrease of L_π is quite limited. The propagation loss can be evaluated in terms of the maximum allowed length $L_{\max}$ as shown in the red curve in Fig. 4(b), indicating the length where the energy at the output decays to $1/e$ of its original value. We would focus our attention on the condition that $L_\pi < L_{\max}$ in which case the waveguide has enough power at the output [20]. It can be seen that almost all the μ_c (as long as $\Delta\mu_c > 0.1$ eV) satisfies this restriction. When $\Delta\mu_c$ = 0.3 eV, L_π is 120 μm, which is one order of magnitude smaller than the present reported value [5–8]. If the width of the modulation arm is 450 nm and the distance between the two arms is 1.7 μm. Taking into account of the electrode width of 1 μm on each arm side, the overall width of the device is 5 μm. thus the footprint of our proposed modulator is only 120 μm×5 μm [20]. It should be mentioned that the arm length can be further reduced if multi-layer graphene is used which is discussed in Section 4. Please note that conventional MZ modulator needs several millimeters to reach the π phase shift. This small size as well as the CMOS compactable structure indicates its valuable capability to be integrated into photonic circuits in a single chip.

Another important parameter for the MZ modulator is the applied voltage V_g. V_g is particularly important to influence the chemical potential of the graphene sheet, because the chemical potential is derived by the voltages of the external electrode which is contacted with graphene sheet following the expression [20]:

$$\mu_c = \hbar V_F \sqrt{\eta\pi \left| (V_g - V_{\text{Dirac}}) \right|}, \tag{5}$$

where $V_F = 3 \times 10^6$ m/s is the Fermi velocity, and $\eta = 9 \times 10^{16}\ \text{m}^{-2}\cdot\text{V}^{-1}$ is estimated from a single capacitor model. Since the voltage offset caused by natural doping V_{Dirac} is a finite number (e.g., 0.8 V in Ref. [3], $V_g - V_{\text{Dirac}}$ can be considered as the applied voltage for simplicity. For the proposed MZI modulator, the two arms are applied with different voltages: one is with the constant voltage V_{g1} which corresponds to μ_{c1} = 1 eV, thus it is called the reference arm; the other is switched between V_{g1} (for signal "1") and V_{g2} (for signal "0") according to the transmitted signals, thus it is called the modulated arm. The blue curves in Fig. 4(c) have shown the calculated applied voltages for the modulated arm, which are much smaller if compared with other modulators. The difference between V_{g1} and V_{g2} is called π shift voltage V_π. As expected, V_π increases when $\Delta\mu_c$ is enlarged. The product between L_π and V_π is known as the modulation efficiency. Since L_π decreases much faster than the increase speed of V_π, the minimum $V_\pi L_\pi$ would be achieved at 55 V·μm where L_π is smallest at 120 μm..

One significant advantage for MZ modulator is that the extinction ratio is high if compared with EA modulators, because the π phase shift between two arms leads to absolute "0" output for the "off" state. Light propagates through the arms experiences different losses at either 8.86 $\text{Im}(n_{\text{eff}})k_0$, and the extinction ratio is thus calculated through

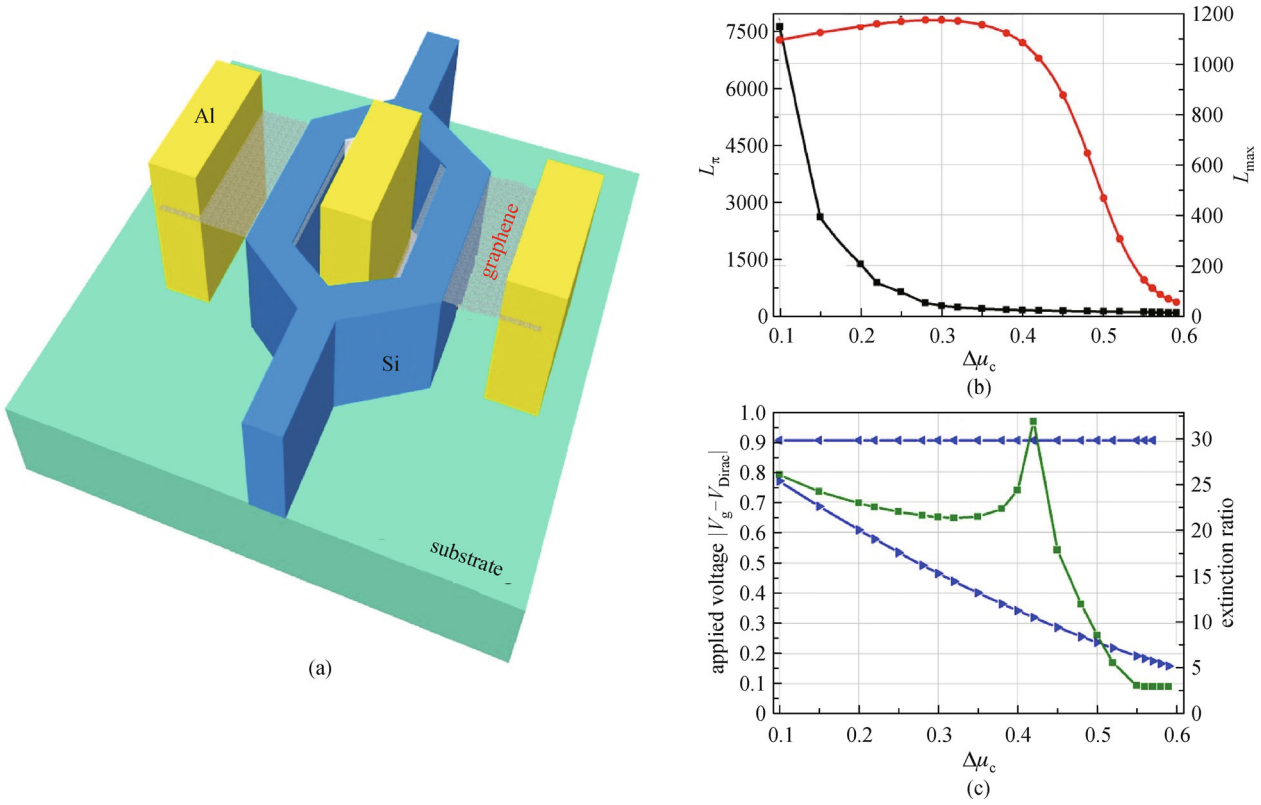

Fig. 4 (a) Schematic pictures for top view of the MZ modulator configuration; (b) relationship between L_π/L_{max} and μ_c; (c) relationship between the applied votages/extinction ratio and μ_c

$$\mathrm{ER} = 10\log\left(T_{\max}/T_{\min}\right) = 20\log\left(\frac{2e^{-\frac{\pi L \mathrm{Im}(n_{\mathrm{eff1}})}{\lambda}}}{e^{-\frac{\pi L \mathrm{Im}(n_{\mathrm{eff1}})}{\lambda}} - e^{-\frac{\pi L \mathrm{Im}(n_{\mathrm{eff2}})}{\lambda}}}\right). \quad (6)$$

The extinction ratio is decided by the choice of $\mathrm{Im}(n_{\mathrm{eff}})$, indicating the possibility of high extinction ratio as long as we take appropriate μ_c. Figure 4(c) shows the extinction ratio and applied voltage V_g variations with μ_c, where a maximum extinction ratio of 34 dB has been observed at $\Delta\mu_c$= 0.42 eV. The obtained high extinction ratio is due to that the $\mathrm{Im}(n_{\mathrm{eff}})$ have been taken the same value under the two modulation states. Furthermore, unlike the semiconductor modulator which has speed limitation posed by the minority carrier lifetime, the graphene modulator has no carrier limitation. Therefore, its bandwidth may be simply evaluated by the resistor capacitor (RC) delay $f_{3\ \mathrm{dB}} = 1/2\pi RC$ formula, indicating a possible larger bandwidth capability.

3.2 Graphene-based electric-absorption modulator

As it is known that the corresponding propagation loss is linked with $\mathrm{Im}(n_{\mathrm{eff}})$, there exists the possibility to modulate the imaginary part of n_{eff} directly to control the propagation loss. Next we discussed how to employ graphene's $\mathrm{Im}(n_{\mathrm{eff}})$ to configure an amplitude (absorption) modulator. A schematic picture of the electric-absorption modulator is constructed as depicted in Fig. 5(a) based on the previous waveguide where the graphene sheet is embedded in the Si-waveguide. When $\mu_c < 0.4$ eV (the inflection point in Fig. 2), the waveguide suffers the larger attenuation. When $\mu_c > 0.4$ eV, the waveguide has lower loss. For the ranges $\mu_c < 0.2$ eV and $\mu_c > 0.4$ eV, the loss stays constant because the $\mathrm{Im}(n_{\mathrm{eff}})$ does not change. Let us fix the chemical potential at μ_c = 0.7 eV where the loss of the proposed modulator is 0.01dB/μm as reference, and the chemical potential gradually decrease. It is found at μ_c = 0.2 eV, the waveguide suffers the largest loss of 0.62 dB/μm. As a result, modulation depth around 0.96 dB can be achieved via the 22.6 μm long waveguide, which is the same magnitude as that reported in Ref. [24]. It should be pointed out that the drawback of absorption modulator is the modulation depth is low if compared with the phase modulator [38], because the output of the modulator cannot be exactly zero. It should be pointed out that for the applications that not emphasize on the extinction ratio, optical absorption modulator is also a good choice since it provide much smaller footprint and lower power consumption.

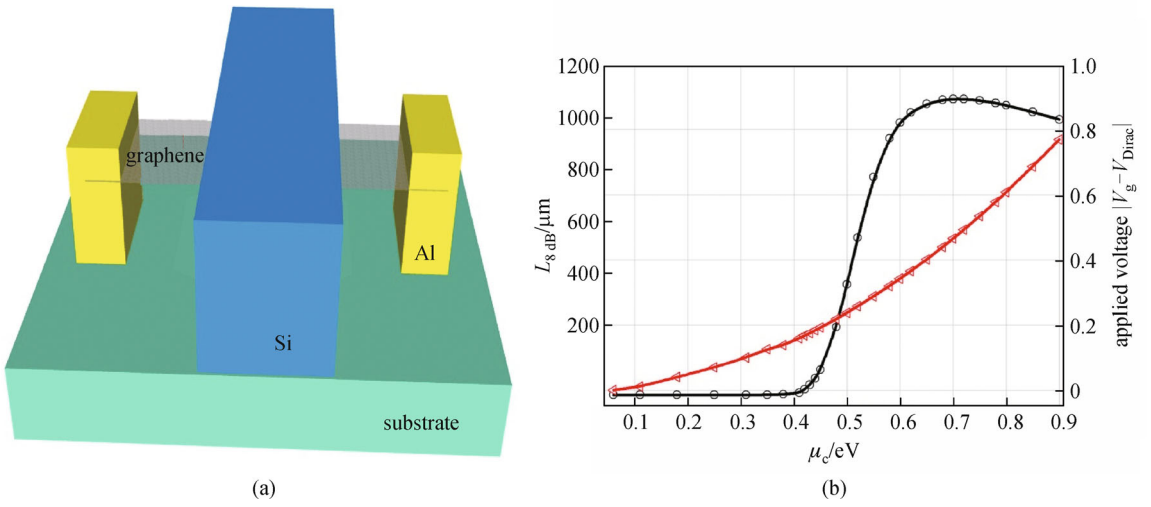

Fig. 5 (a) Schematic pictures for the absorption modulator configuration; (b) relationship between $L_{8\ dB}$ and μ_c

The width of the GESW is 450 nm, the distance between the electrode and the ridge of the waveguide is 1.275 μm and the length is 22.6 μm. Furthermore, taking the length of each electrode for 1 μm, the total width of the waveguide is 5 μm, thus the size of this EA modulator is 113 μm^2, which is much smaller compared to the previous reported modulators [5–8].

For the modulator with the above parameters, the equivalent capacitance and the overall resistance are estimated to be 80 pF and 12 Ω, respectively [39]. The predicted bandwidth for the proposed modulator is estimated by the following expression: $f_{3\ dB} = 1/2\pi RC$ [39], thus the bandwidth of the modulator is estimated up to 207 GHz. Under the ideal situation with zero noise in a communication system, the signal speed can be estimated by the Nyquist-Shannon Law: $B = 2W$, where B is signal speed in binary element data format and W represents the bandwidth. Then the modulation speed for the proposed modulator can be evaluated to 414 Gbit/s in binary element data format.

3.3 Comparison between isotropic and anisotropic graphenes

At the early stage of research, graphene was treated as isotropic material. At the ENZ point where the permittivity of graphene is approaching zero and graphene sheet transfers from dielectric-like to metallic-like, the results in Refs. [24,37] showed that strong n_{eff} variation should occur, as shown in Fig. 6(a). In this case, both Re(n_{eff}) and Im(n_{eff}) have unexpected symmetries toward the ENZ point. Re(n_{eff}) displays an odd-symmetry toward the ENZ point, while Im(n_{eff}) displays an even-symmetry. Figure 6 (b) exhibits the corresponding electric field profile when μ_c= 0.513 eV (ENZ point), where most of the electric fields are confined inside the graphene sheet. Recently, some researchers have realized that graphene is actually an anisotropic material [20,32], and a linear relation between graphene's in-plane permittivity and effective mode index can be observed, as discussed in above sessions and depicted in Fig. 3. Figure 6(d) showed the corresponding electric field distribution for the transverse electric (TE) polarizations.

To compare the differences between the two cases, the electric fields when graphene is treated as isotropic and anisotropic are depicted in Figs. 6(b) and 6(d). Figure 6(b) depicts the electric field distribution where the transverse-magnetic field (TM) is studied and graphene is treated as isotropic material. Therefore, its electric field polarized in the vertical direction changes with the chemical potentials, and $\varepsilon_\perp$ is tunable. At the ENZ point, most of the electric fields are strongly confined inside the graphene layer, thus they can feel $\varepsilon_\perp$ variation of graphene. As a result, the waveguide mode distribution changes drastically at the ENZ point and the corresponding n_{eff} changes intensively. This is why the previous references recorded intensive n_{eff} variation at the ENZ point [24,37]. However, Fig. 6(c) shows the situation when graphene is treated as anisotropic material. As only $\varepsilon_{//}$ (not $\varepsilon_\perp$) can be tuned by the chemical potentials, the transverse-electric filed (TE) is considered here whose electric field is polarized along the silicon-graphene interface. The electric fields are observed to fulfill into waveguide region in the form of a Guassian distribution, spreading inside and outside the graphene sheet. According to the boundary condition, the tangent parts of electric fields in the two media must be equal at the interface. Thus the electric field inside and outside the graphene must be continuous along the interface. Therefore, the overall mode displays a Guassian distribution just like a conventional TE mode waveguide does (as there is no graphene embedded).

It should be concluded that because graphene's

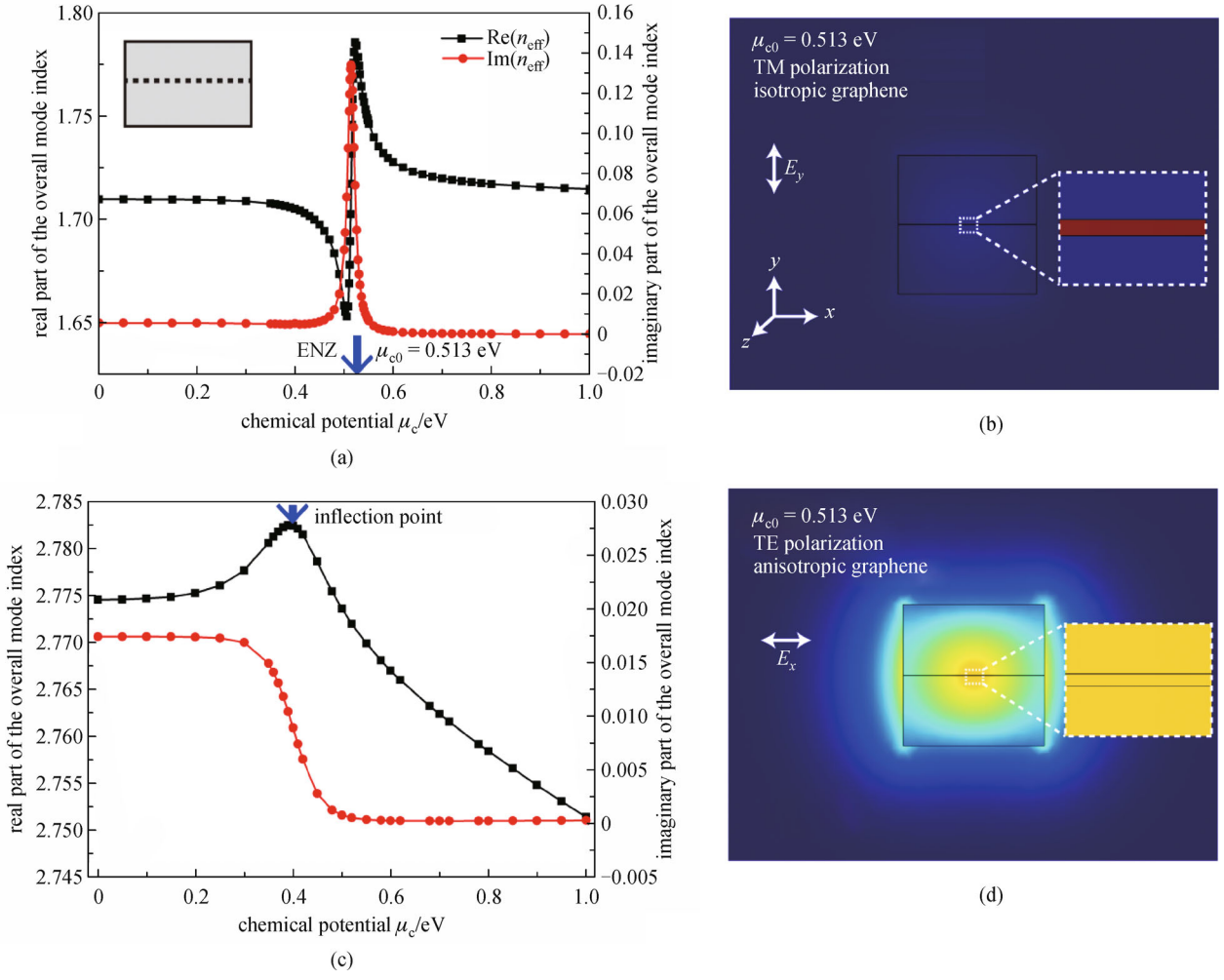

Fig. 6 Transverse magnetic (TM) polarization where graphene is assumed as isotropic: (a) real and imaginary part of effective modal index variation under different chemical potentials; (b) electric field distribution at μ_c = 0.513 eV; transverse electric (TE) polarization where graphene is assumed as anisotropic; (c) real and imaginary part of effective modal index variation under different chemical potentials; (d) electric field distribution at μ_c = 0.513 eV (reprinted from Ref. [20])

periodicity is only in the 2D lattice plane, its tunability should be only inside this plane. In other words, graphene shows anisotropic material properties: the in-plane permittivity ($\varepsilon_{//}$) can be actively tuned by the chemical potentials (the Fermi level), whereas the out-of-plane permittivity ($\varepsilon_{\perp}$, in the direction perpendicular to the graphene sheet) does not vary with the external parameters.

4 Multi-layer graphene-based modulator

4.1 Multi-layer graphene-based modulator

Multi-layer graphene based devices have also been studied for the modulator application. Based on the above monolayer graphene-embedded modulator, it is straightforward to embed the multi-layer graphene sheets inside silicon waveguide. An eight-layer graphene embedded MZ modulator [20] is shown in Fig. 7(a). The corresponding electric field distribution in one of the arms of modulator is shown in Fig. 7(b). As demonstrated previously, the field profile displays a Gaussian-like distribution. It has been theoretically demonstrated that by embedding multi-layer graphene in the silicon waveguide, the Δn_{eff} has been increased significantly under the same chemical potential change compared with the monolayer graphene. Therefore, the L_π has been reduced to 27.57 μm which means a much smaller arm length is needed to acquire the π phase shift, as shown in Fig. 7(c). The overall footprint is then estimated as 5 μm × 30 μm. Moreover, the proposed graphene embedded modulator is highly tunable whose overall modal index is in linear relationship with the in-plane permittivity of graphene. The high modulation efficiency is further optimized to 20 V·μm, which is 6 times better than the monolayer case. In Fig. 7(d), The extinction ratio is 35 dB at smaller arm length compared with Fig. 4.

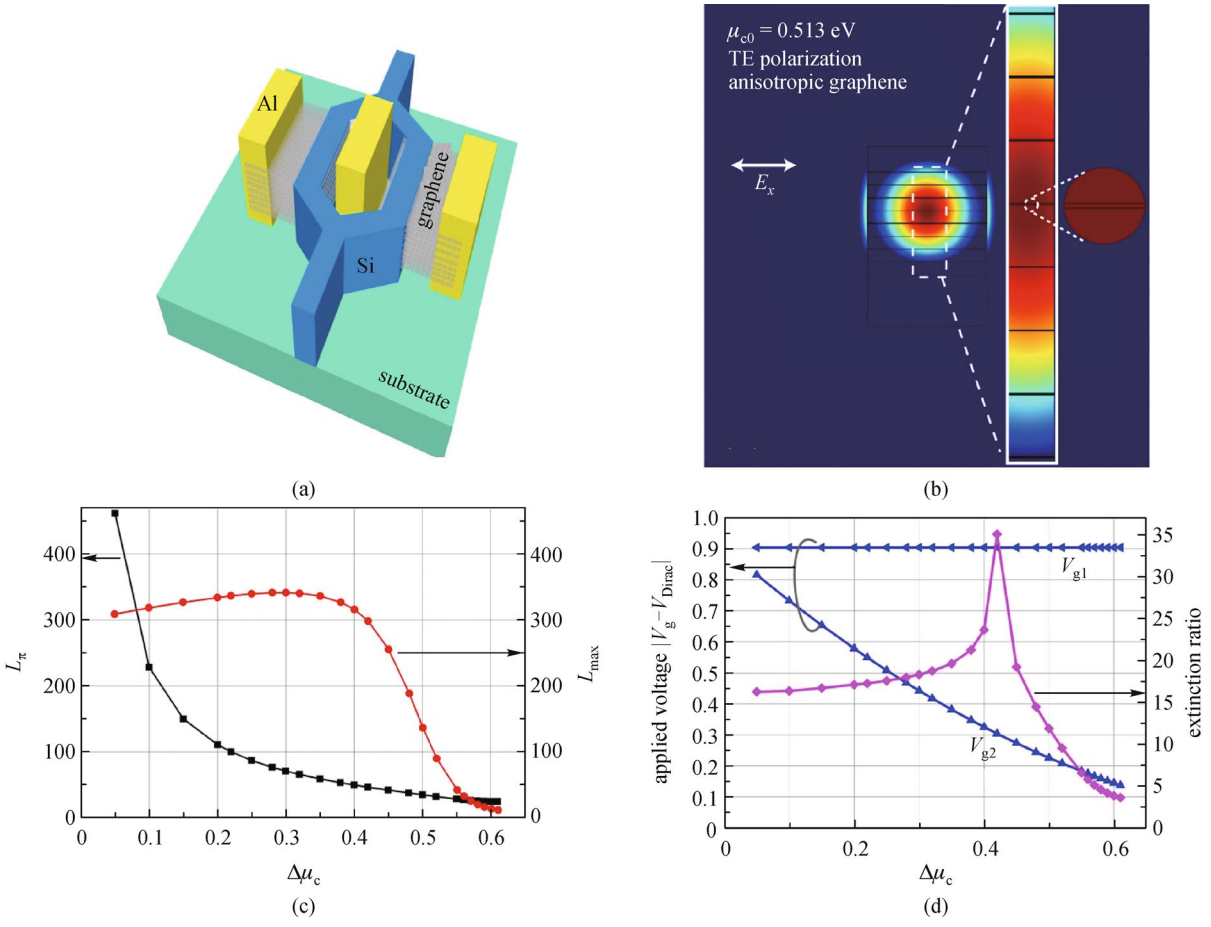

Fig. 7 (a) Schematic pictures for eight-layer graphene embedded MZ modulator configuration; (b) corresponding electric field distribution in one of the arm; (c) relationship between L_π/L_{max} and $\Delta\mu_c$; (d) relationship between the applied votages/extinction ratio and $\Delta\mu_c$ (reprinted from Ref. [20])

Similarly, it is also possible to configure an optical-absorption modulator by embedding multi-layer graphene sheets inside. It is expected the multi-layer absorption modulator will have a shorter arm length and better modulation performance compared with monolayer case, because the light-graphene interaction is enhanced.

4.2 Few-layer graphene-based modulator

Previous discussion on multi-layer graphene relies on the fact that graphene sheets are inserted into the silicon waveguide individually, separated with a distance between the adjacent sheets. However, this scheme adds the difficulties in fabrication and the modulation efficiency is not the best. There is an alternative way to embed an N-layer thick graphene sheet in the silicon waveguide. Particularly, when the number of layer $N < 5$, it is called few-layer graphene that exhibits even better performance than the monolayer graphene. According to the semi-classical model, the few-band effects caused by interlayer coupling can be ignored for few-layer graphene, as experimentally verified in Ref. [40]. When the number of layer $N < 5$, the conductivity of N-layer structure is N times of monolayer graphene's conductivity: $\sigma_N = N \times \sigma_0$ [40,41]. On the other hand, the effective thickness of N-layer structure is $d_N = N \times d_0$ [40,41]. As a result, the in-plane permittivity of few-layer graphene can be also obtained from $\varepsilon(\omega) = 1 + i\sigma(\omega)/(\varepsilon_0\omega\Delta)$. Please note graphene is a kind of anisotropic material, thus the permittivity above is only in the two-dimensional lattice plane. In the direction perpendicular to the lattice plane, the permittivity $\varepsilon_\perp$ is a constant of 2.5 that is same as graphite.

The effective mode index curves for monolayer GESW, two separated monolayer GESW, and bi-layer GESW are plotted in Figs. 8(a) and 8(b). First, the variation of Re(n_{eff}) for the bi-layer GESW is roughly two times of the monolayer GESW as expected. However, the variation of Re(n_{eff}) for the bi-layer GESW is much larger than that of the two separated monolayer GESW, which implies the light-matter interaction between light and bi-layer graphene is much more pronounced compared to that of the two separated monolayer graphene. Secondly, these three

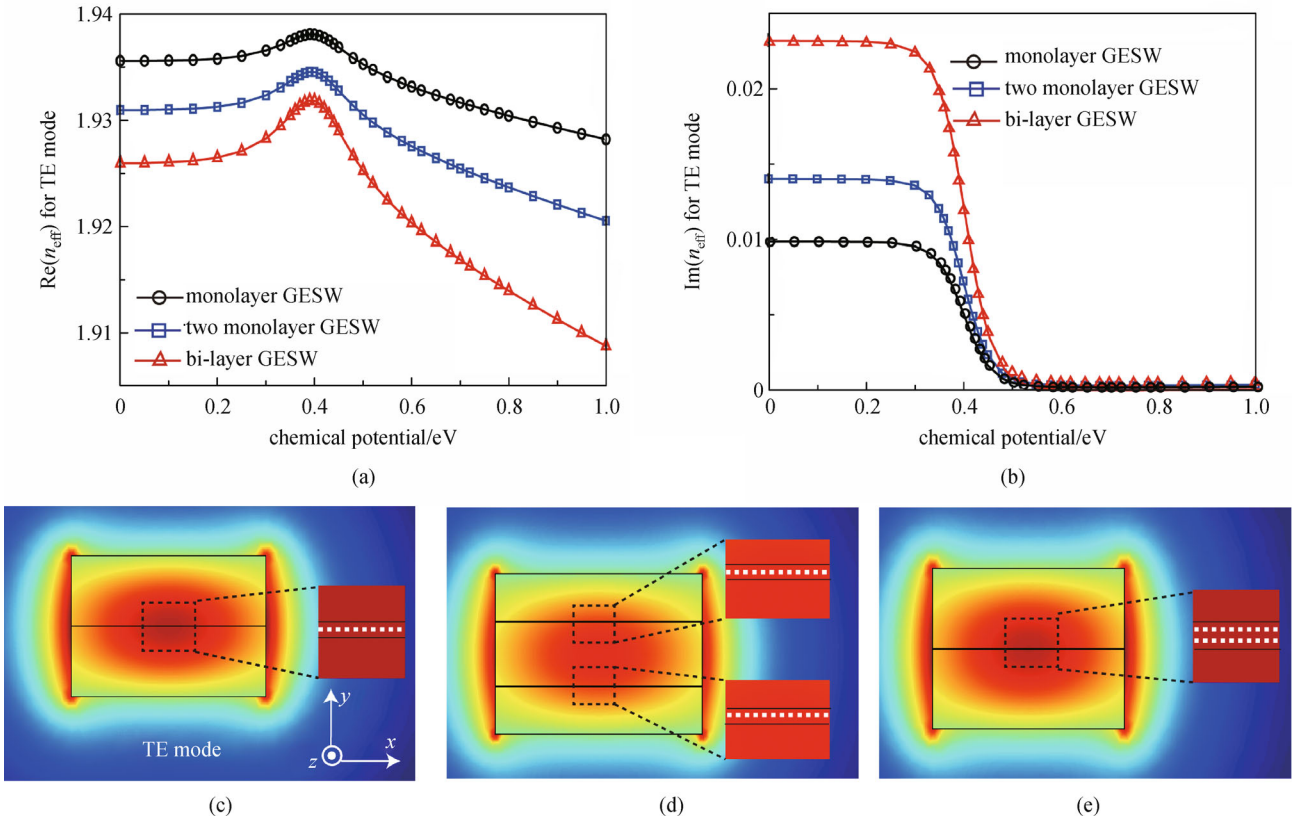

Fig. 8 (a) Re(n_{eff}) with chemical potential variation for monolayer, two separated monolayer, and bi-layer GESW; (b) Im(n_{eff}) with chemical potential variation for monolayer, two separated monolayer, and bi-layer GESW; (c), (d) and (e) represent the electric field distribution for TE polarization mode of monolayer, two separated monolayer, and bi-layer GESW under chemical potential of 0 eV, respectively (reprinted from Ref. [32])

curves have basically the same variation trend, namely, it first increases to a maximum value (around the chemical potential of 0.4 eV) and then decreases to the minimum value (at the chemical potential of 1 eV). Therefore, a large Δn_{eff} can be obtained when chemical potential is between 0.4 and 1 eV. In addition, since graphene is a highly tunable material, its chemical potential (the Fermi level) can be varied with the applied gate-voltage. As a result, one could generate the desired n_{eff} by easily controlling the applied gate-voltage. To show the difference, the typical electric field modal profiles for monolayer, two separated monolayer, and bi-layer GESW under chemical potential of 0 eV are plotted in Figs. 8(c) – 8(e), respectively.

Figure 9 depicts the relationship between Δn_{eff} and the number of embedded graphene layer [32]. A linear relationship between Δn_{eff} and the number of embedded graphene layer N is obtained. The inset of Fig. 9 depicts the ratio k_g/k_{total} under different number of embedded graphene layer N, showing that the light-matter interaction is proportional to N. In particular, the maximum Δn_{eff} for bi-layer, tri-layer, and quadri-layer GESW is 0.0231, 0.033, and 0.047, respectively. According to the equation $\Delta\varphi = (2\pi/\lambda) \times \Delta n_{eff} \times L$, the phase of the incident light will experience a corresponding change after propagating through a certain length. As for the quadri-layer GESW, a calculated length L_π of only 16.5 μm is required to achieve a 180° phase shift. Compared to the conventional silicon waveguide (Δn_{eff} is only at the level of 10^{-4} and the required length L_π to achieve π shift will be several millimeters) the arm length of the proposed quadri-layer GESW has decreased two orders of magnitude.

4.3 Influences of wavelength and temperature

All previous results are obtained at the incident wavelength of 1550 nm. To figure out the stability of the phase modulation ability, we studied Δn_{eff} under different operating wavelengths as illustrated in Fig. 10(a). It can be seen that red square line depicts maximum Δn_{eff} as a function of wavelength while black circle line exhibits the phase modulation ability, which can be quantified by the required length L_π to reverse the phase of incident light. By sweeping the wavelength from 1520 to 1580 nm, maximum Δn_{eff} is almost unchanged. In other words, the phase modulation ability remains stable in a large range of the incident wavelength (60 nm). To put it more specifically,

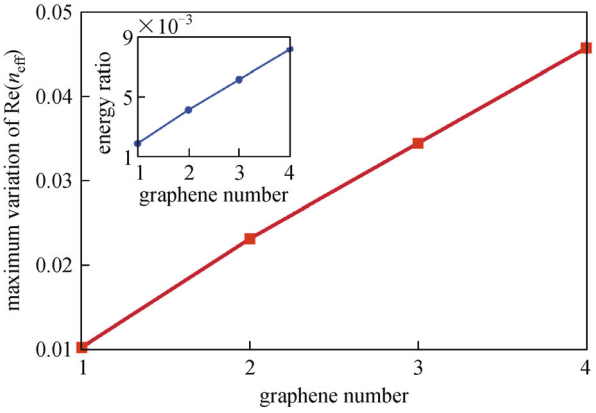

Fig. 9 Maximum variation of Re(n_{eff}) as function of the number of graphene layer; the inset depicts the energy ratio k_g/k_{total} (reprinted from Ref. [32])

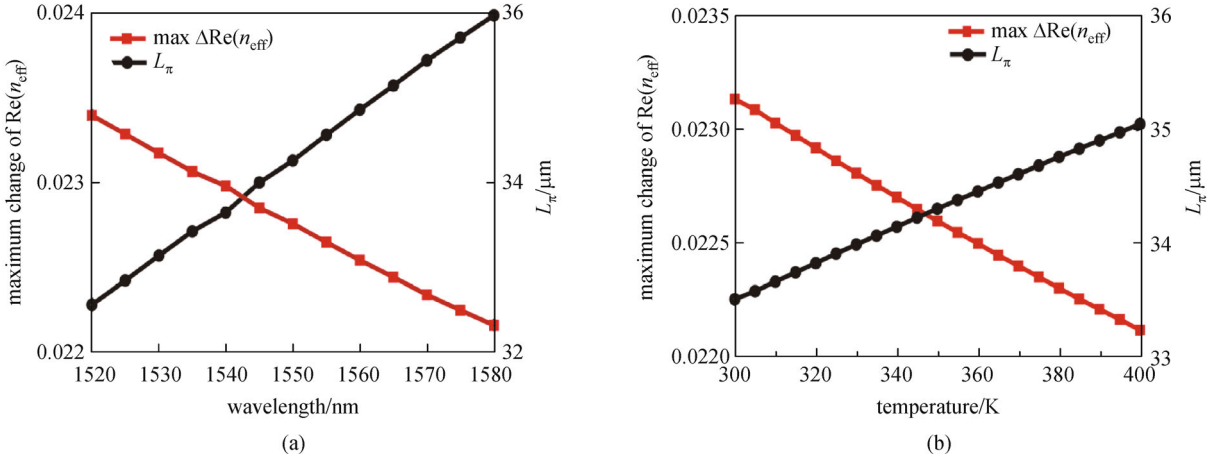

Fig. 10 (a) Red line depicts the maximum variation Re(n_{eff}) as function of incident light wavelength and black line depicts the required length L_π as function of incident light wavelength; (b) red line depicts the maximum variation Re(n_{eff}) as function of temperature and black line depicts the required length L_π as function of temperature (reprinted from Ref. [32])

maximum Δn_{eff} is 0.0223, 0.0231 and 0.0239, respectively and the required length L_π is 34.8, 33.5 and 32.3 μm, respectively at 1520, 1550 and 1580 nm. It is concluded that modulation phase ability of the proposed waveguide exhibits a good tolerance under a slight fluctuation of the incident wavelength.

The temperature influence on the proposed modulator is also studied. Considering a typical server/personal commputer system is often operated at a temperature around 70°C and the temperature will have a fluctuation during the working process. In this case, typically thermo-electric controllers are required to maintain the stabilization of the temperature if the properties of the electro-optical devices are temperature-sensitive. This is why the phase modulation ability is investigated in a large range of the temperature (300 to 400 K). The maximum Δn_{eff} as a function of temperature and the required length L_π of the waveguide as a function of temperature are shown as the red square line and black circle line in Fig. 10(b), respectively. The results in Fig. 10(b) indicate that although we sweep the temperature span from 300 to 400 K, the phase modulation ability still remains stable. More precisely, the maximum Δn_{eff} is 0.0231, 0.0226 and 0.0221 at the temperature of 300, 350 and 400 K, respectively. It can be concluded that the performance of the proposed waveguide can still sustain a high level despite that the outside temperature experiences a large fluctuation, such property makes it possible to work in a rigorous environment.

It should be also mentioned that the carrier mobility of few-layer graphene is slower compared to the monolayer graphene. Because the resistance and response time of the proposed modulator are proportional to the carrier mobility, the slower carrier mobility in our proposed few-layer GESW will reduce the modulation speed and increase the energy consumption compared to the mono-

layer GESW. The modulation speed is limited by the RC delay: $f_{3\,\mathrm{dB}} = 1/2\pi RC$, e.g., if the effective resistance is 200 Ω and capacitance is taken as 40 fF, the modulation speed is estimated about only 40 Gbit/s. In addition, the proposed modulator can only work under TE polarization. The polarization-independent modulator is needed in future studies.

5 Graphene-based fiber modulator

All above designs imply the advantages to integrate graphene into silicon substrate, but for a more popular usage such as the widely used fiber-optic communication systems, the previous design may be not appropriate due to the large insertion/coupling loss and strong backward scattering caused by adding external components into the fiber. Attentions have also been paid to the graphene-based fiber modulator. One significant advantage of merging graphene with fiber system is the possibility to achieve broadband all-optical modulation. Meanwhile, the high-speed operation (up to 500 GHz) can be obtained in a graphene-based fiber modulator due to ultrafast photo carrier generation and relaxation (variation of the probe and pump signals as a function of time with modulation frequencies) [42].

In this section, we reviewed two kinds of all-optical modulators based on graphene.

Tian et al. have reported a graphene covered microfiber modulator as shown in Fig. 11 [43]. The microfiber is sandwiched between low refractive index magnesium fluoride (MgF_2) substrate and Polydimethylsiloxane (PDMS) supported graphene film. Microfibers have many fascinating features such as flexible configurability, strong confinement and large evanescent fields, and it can be easily coupled to each other or other optical material with low loss. The microfibers are drawn from a conventional single mode fiber by use of a flame-brushing technique, with a diameter of down to 8 μm, a length of up to 1 cm, and a low insertion loss of down to 0.1 dB. The graphene sample was synthesized by a chemical vapor deposition growing on polycrystalline Cu substrate, and a new dry transfer method was used to avoid the impact of contamination on light guiding. In their design, they used a two-layer-composite-structure of polyethylene terephthalate and silica gel was applied to transfer single-layer and bi-layer graphene from the copper substrate to the PDMS.

A continuous wave (CW) pump laser at 1060 nm was coupled into the graphene to excite the optical nonlinearities of graphene films while the signal laser is at 1550 nm. As the excitation is increased to higher intensity, the photo generated carriers increase in concentration, and saturated absorption or absorption bleaching is achieved due to the Pauli blocking process. Therefore, along with the pump light excitation, the absorption of broadband CW probe light in the graphene-covered micro-fiber will decrease due to the effect of saturated absorption. The modulation depths are roughly 5 and 13 dB for single-layer and bi-layer graphene films, respectively. The modulator in Fig. 11 can work under room temperature with fast carrier mobility through the band-filling effect with pump excitation.

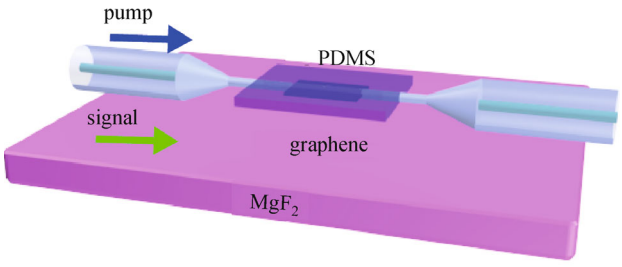

Fig. 11 Schematic of the graphene-covered-microfiber structure. The microfiber is sandwiched between low refractive index MgF_2 substrate (with a refractive index of 1.37 at 1.55 μm) and PDMS-supported graphene film

A similar graphene-based fiber modulator is also proposed by Tong's group in Zhejiang University called graphene-clad fiber all-optical modulator [44], as illustrated in Fig. 12. The difference between the two graphene-based fiber modulators is that Tong et al. used a subwavelength diameter fiber (the diameter of the subwavelength is around 1 μm for single-mode operation in C-band of optical communication which is much smaller than the conventional microfiber diameter around 10 μm). In their design, a thin layer of graphene was wrapped around a single-mode microfiber, which was a section with the ends tapered down from a standard telecom optical fiber.

When there is no pump light, a weak infrared signal wave coupled into the modulator experiences significant attenuation due to absorption in graphene as it propagates along. When a switch light is introduced, it excites carriers in the graphene and through Pauli blocking of interband transitions it shifts the absorption threshold of graphene to higher frequency, resulting in a much lower attenuation of the signal wave. The switch light leads to modulation of the signal output from the fiber, and its response time is limited by the relaxation of the excited carriers. The relaxation time of carrier–carrier scattering in graphene is known to be tens to hundreds of femtoseconds and that of carrier-phonon scattering ~1 to a few picoseconds. The switch-light-induced refractive index change of the atomically thin graphene is small enough that it does not appreciably change the wave-guiding mode of the microfiber. In the experiment performed by Tong et al. [44], the graphene-based microfiber modulator can achieve a modulation depth of 38% and a response time of ~2.2 ps.

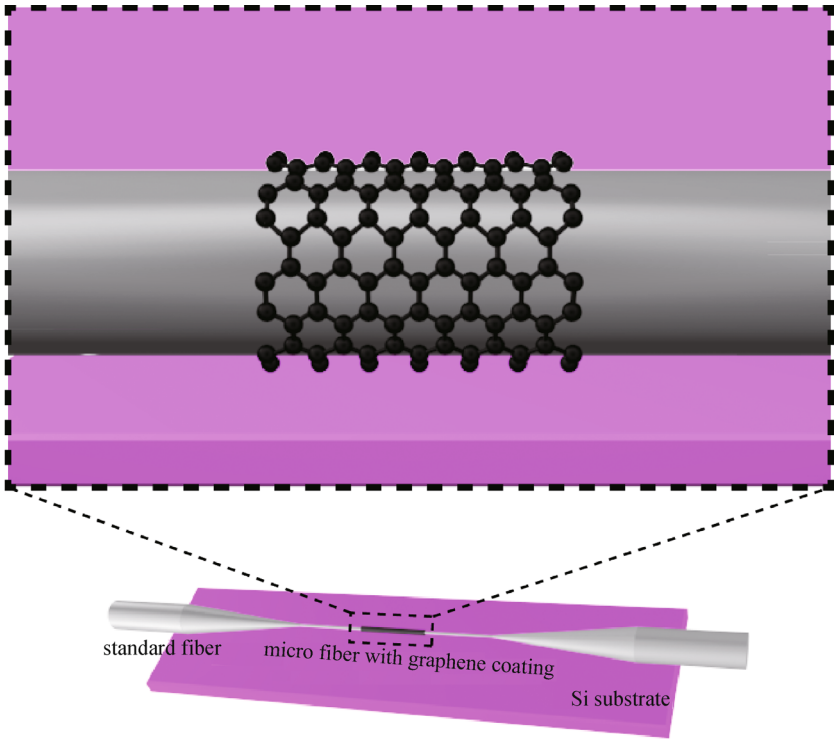

Fig. 12 Schematic illustration of a graphene coated optical fiber modulator. A thin layer of graphene is wrapped around a microfiber that is a section tapered down from a standard telecom optical fiber (reprinted from Ref. [44])

6 Conclusion

In conclusion, we reviewed recent progress in graphene-based optical modulators. By embedding the graphene sheet into the silicon waveguide, the light-matter interaction has been significantly enhanced: the overall mode index, Re(n_{eff}) and Im(n_{eff}), are linked to the in-plane permittivity of the embedded graphene and the n_{eff} variation of GESW can be orders of magnitude larger than silicon waveguide. The modulators based on single-layer graphene, bi-layer graphene, eight-layer graphene, and few-layer graphene were investigated and categorized. The isotropic material property and anisotropic material property were compared. The influences of wavelength, temperature, number of layer N were studied. The recent graphene-based fiber modulators were also reviewed. It can be concluded that graphene is a very promising material for enhancing the modulation effect in silicon, and has great potentials for future CMOS compatible high efficiency optical modulator, showing significant influence for optical interconnects in future integrated optoelectronic systems. The high modulation efficiency as well as ultrafast speed modulation suggests the valuable perspective for utilizing graphene optics in nanophotonic circuits.

Acknowledgements This work was supported by the National Basic Research Program of China (No. 2014CB340005), the National Natural Science Foundation of China (Grant Nos. 61205054 and 61371029), Zhejiang Provincial Natural Science Foundation of China (Nos. Z1110330 and LQ12F05006), the Excellent Young Faculty Awards Program (Zijin Plan) at ZhejiangUniversity.

References

1. Jalali B, Fathpour S. Silicon photonics. Journal of Lightwave Technology, 2006, 24(12): 4600–4615
2. Li E P, Chu H S. Plasmonics Nanoelectronics and Sensing Devices. Cambridge: Cambridge University Press, 2014
3. Liu M, Yin X, Ulin-Avila E, Geng B, Zentgraf T, Ju L, Wang F, Zhang X. A graphene-based broadband optical modulator. Nature, 2011, 474(7349): 64–67
4. Tu X, Liow T Y, Song J, Luo X, Fang Q, Yu M, Lo G Q. 50-Gb/s silicon optical modulator with traveling-wave electrodes. Optics Express, 2013, 21(10): 12776–12782
5. Thomson D, Gardes F Y, Fedeli J M, Zlatanovic S, Hu Y, Kuo B P P, Myslivets E, Alic N, Radic S, Mashanovich G Z, Reed G T. 50-Gb/s silicon optical modulator. IEEE Photonics Technology Letters, 2012, 24(4): 234–236
6. Baba T, Akiyama S, Imai M, Hirayama N, Takahashi H, Noguchi Y, Horikawa T, Usuki T. 50-Gb/s ring-resonator-based silicon modulator, Optical Express, 2013, 21(10): 11869–11876
7. Thomson D J, Gardes F Y, Cox D C, Fedeli J M, Mashanovich G Z, Reed G T. Self-aligned silicon ring resonator optical modulator with focused ion beam error correction. Journal of the Optical Society of America B, 2013, 30(2): 445–449
8. Tang Y, Peters J D, Bowers J E. Over 67 GHz bandwidth hybrid

silicon electroabsorption modulator with asymmetric segmented electrode for 1.3 μm transmission. Optics Express, 2012, 20(10): 11529–11535
9. Smirnova D A, Gorbach A V, Iorsh I V, Shadrivov I V, Kivshar Y S. Nonliear swithing with a graphene coupler. Physical Review B: Condensed Matter and Materials Physics, 2013, 88(4): 045443
10. Kim K, Cho S H, Lee C W. Nonlinear optics: graphene-silicon fusion. Nature Photonics, 2012, 6(8): 502–503
11. Lee C C, Suzuki S, Xie W, Schibli T R. Broadband graphene electro-optic modulators with sub-wavelength thickness. Optics Express, 2012, 20(5): 5264–5269
12. Sensale-Rodriguez B, Yan R, Kelly M M, Fang T, Tahy K, Hwang W S, Jena D, Liu L, Xing H G. Broadband graphene terahertz modulators enabled by intraband transitions. Nature Communications, 2012, 3(4): 780
13. Grigorenko A N, Polini M, Novoselov K S. Graphene plasmonics. Nature Photonics, 2012, 6(11): 749–758
14. Vakil A, Engheta N. Transformation optics using graphene. Science, 2011, 332(6035): 1291–1294
15. Bao Q, Loh K P. Graphene photonics, plasmonics, and broadband optoelectronic devices. ACS Nano, 2012, 6(5): 3677–3694
16. Hao R, Cassan E, Xu Y, Qiu M, Wei X C, Li E P. Reconfigurable parallel plasmonic transmission lines with nanometer light localization and long propagation distance. IEEE Journal of Selected Topics in Quantum Electronics, 2013, 19(3): 460189
17. Hao R, Li E, Wei X. Two-dimensional light confinement in cross-index-modulation plasmonic waveguides. Optics Letters, 2012, 37 (14): 2934–2936
18. Auditore A, de Angelis C, Locatelli A, Aceves A B. Tuning of surface plasmon polaritons beat length in graphene directional couplers. Optics Letters, 2013, 38(20): 4228–4231
19. Zhu X, Yan W, Mortensen N A, Xiao S. Bends and splitters in graphene nanoribbon waveguides. Optics Express, 2013, 21(3): 3486–3491
20. Hao R, Du W, Chen H, Jin X, Yang L, Li E. Ultra-compact optical modulator by graphene induced electro-refraction effect. Applied Physics Letters, 2013, 103(6): 061116
21. Li Z, Yu N. Modulation of mid-infrared light using graphene-metal plasmonic antennas. Applied Physics Letters, 2013, 102(13): 131108
22. Andersen D R. Graphene-based long-wave infrared TM surface plasmon modulator. Journal of the Optical Society of America B, Optical Physics, 2010, 27(4): 818–823
23. Grigorenko A N, Polini M, Novoselov K S. Graphene plasmonics. Nature Photonics, 2012, 6(11): 749–758
24. Lu Z, Zhao W. Nanoscale electro-optic modulators based on graphene-slot waveguides. Journal of the Optical Society of America B, Optical Physics, 2012, 29(6): 1490–1496
25. Mikhailov S A, Ziegler K. New electromagnetic mode in graphene. Physical Review Letters, 2007, 99(1): 016803
26. Jablan M, Buljan H, Soljačić M. Plasmonics in graphene at infrared frequencies. Physical Review B: Condensed Matter and Materials Physics, 2009, 80(24): 245435
27. Gan C H, Chu H S, Li E P. Synthesis of highly confined surface plasmon modes with doped graphene sheets in the midinfrared and terahertz frequencies. Physical Review B: Condensed Matter and Materials Physics, 2012, 85(12): 125431
28. Ju L, Geng B, Horng J, Girit C, Martin M, Hao Z, Bechtel H A, Liang X, Zettl A, Shen Y R, Wang F. Graphene plasmonics for tunable terahertz metamaterials. Nature Nanotechnology, 2011, 6 (10): 630–634
29. Fei Z, Rodin A S, Andreev G O, Bao W, McLeod A S, Wagner M, Zhang L M, Zhao Z, Thiemens M, Dominguez G, Fogler M M, Castro Neto A H, Lau C N, Keilmann F, Basov D N. Gate-tuning of graphene plasmons revealed by infrared nano-imaging. Nature, 2012, 487(7405): 82–85
30. Chen J, Badioli M, Alonso-González P, Thongrattanasiri S, Huth F, Osmond J, Spasenović M, Centeno A, Pesquera A, Godignon P, Elorza A Z, Camara N, García de Abajo F J, Hillenbrand R, Koppens F H. Optical nano-imaging of gate-tunable graphene plasmons. Nature, 2012, 487(7405): 77–81
31. Gusynin V P, Sharapov S G, Carbotte J P. Magneto-optical conductivity in graphene. Journal of Physics: Condensed Matter, 2007, 19(2): 026222
32. Du W, Hao R, Li E P. The study of few-layer graphene based Mach-Zehnder modulator. Optics Communications, 2014, 323: 49–53
33. Gosciniak J, Tan D T. Graphene-based waveguide integrated dielectric-loaded plasmonic electro-absorption modulators. Nanotechnology, 2013, 24(18): 185202
34. Lin H, Pantoja M F, Angulo L D, Alvarez J, Martin R G, Garcia S G. FDTD modeling of graphenedevices using complex conjugate dispersion material model. IEEE Microwave and Wireless Components Letters, 2012, 22(12): 612–614
35. Wang B, Zhang X, Yuan X, Teng J. Optical coupling of surface plasmons between graphene sheets. Applied Physics Letters, 2012, 100(13): 131111
36. Li H, Wang L, Huang Z, Sun B, Zhai X, Li X. Mid-infrared, plasmonic switches and directional couplers induced by graphene sheets coupling system. Europhysics Letters, 2013, 104(3): 37001
37. Yang L, Hu T, Hao R, Qiu C, Xu C, Yu H, Xu Y, Jiang X, Li Y, Yang J. Low-chirp high-extinction-ratio modulator based on graphene-silicon waveguide. Optics Letters, 2013, 38(14): 2512–2515
38. Barnes W L, Dereux A, Ebbesen T W. Surface plasmon subwavelength optics. Nature, 2003, 424(6950): 824–830
39. Kim K, Choi J Y, Kim T, Cho S H, Chung H J. A role for graphene in silicon-based semiconductor devices. Nature, 2011, 479 (7373): 338–344
40. Bao Q, Zhang H, Wang B, Ni Z, Lim C H Y X, Wang Y, Tang D Y, Loh K P. Broadband graphene polarizer. Nature Photonics, 2011, 5(7): 411–415
41. Ni Z H, Wang H M, Kasim J, Fan H M, Yu T, Wu Y H, Feng Y P, Shen Z X. Graphene thickness determination using reflection and contrast spectroscopy. Nano Letters, 2007, 7(9): 2758–2763
42. Zhou F, Hao R, Jin X, Zhang X, Li E. A Graphene-enhanced fiberoptic phase modulator with large linear dynamic range. IEEE Photonics Technology Letters, 2014 (accepted)
43. Liu Z B, Feng M, Jiang W S, Xin W, Wang P, Sheng Q W, Liu Y G, Wang D N, Zhou W Y, Tian J G. Broadband all-optical modulation using a graphene-covered-microfiber. Laser Physics Letters, 2013, 10(6): 065901

44. Li W, Chen B, Meng C, Fang W, Xiao Y, Li X, Hu Z, Xu Y, Tong L, Wang H, Liu W, Bao J, Shen Y R. Ultrafast all-optical graphene modulator. Nano Letters, 2014, 14(2): 955–959

Ran Hao (M'11) received his Ph.D. degree in physics from University Paris XI, France in December, 2010. And he received his second Ph.D. degree in photonics from Wuhan National Laboratory for optoelectronics, Huazhong University of Science & Technology, China in 2011. He is currently an assistant professor in Department of Information Science & Electronic Engineering, Zhejiang University, China. He has won the Distinguished Young Scholar Award in 2011 and the Excellent Young Faculty Awards Program (Zijin Plan) in 2012 at Zhejiang University. His current research interests include nanoplasmonics, nanophotonics, nanofabrication, photonic crystals, slow light phenomena and graphene photonics. He has published more than 35 international journal papers and more than 20 international conference papers in the field of photonics. Dr. Hao is a member of the Optical Society of America and a member of IEEE.

Jiamin Jin receieved her Bachelors degree with specialization in communication engineering from Communication University of China, Beijing, China, in 2012. She is currently pursuing a Masters degree at Zhejiang University, Hangzhou, China. Her research interests are focused on graphene based modulator and wideband graphene slow light waveguide.

Xingchang Wei (M'01-SM'09) received the Ph.D. degree in electrical engineering from Xi'an University of Electronic Science and Technology, China, in 2001. From 2001 to 2010, he has been with the ASTAR Institute of High Performance Computing, Singapore, as a research fellow, senior research engineer, and then a research scientist. He joined Zhejiang University, Hangzhou, China, as a full professor in 2010. His main research interests include 3D IC analysis, power integrity and signal integrity simulation and design, EMC modelling and simulation, and the development of fast algorithms for computational electromagnetics.

He authored over 40 papers published in prestigious international journals and conferences. He was the recipient of the 2007 Singapore IES (Institution of Engineers) Prestigious Engineering Achievement Award for his contribution on the development of a novel electromagnetic compatibility simulation facility. He was the Co-Chair of Technical Program Committee of 2010 IEEE Electrical Design of Advanced Packaging & Systems Symposium.

Xiaofeng Jin received the B.S. degree in optical engineering from Huazhong University of Science and Technology, Wuhan, China, in 1990, the M.S. degree in underwater acoustic engineering from China Ship Building Institute, Jiangsu, China, in 1993, and the Ph.D. degree in optical engineering from Zhejiang University, Hangzhou, China, in 1996. In 1999, he was appointed as an associate professor at Department of Information and Electronic Engineering, Zhejiang University and full professor, in 2006. His current research interests include microwave photonics, photonic circuits, components and modules, and smart sensing systems.

Xianmin Zhang (M'07) received the B.S. and the Ph.D. degrees in physical electronics and optoelectronics, respectively. He was appointed as an associate professor of information and electronic engineering at Zhejiang University, Hangzhou, China, in 1994 and full professor, in 1999. He is currently the Chair of Department of Information Science and Electronic Engineering, Zhejiang University. His research interests include microwave photonics, optic fiber, and optic communication.

Erping Li (S'91, M'92, SM'01, F'08) received his Ph.D. degree from Sheffield, U.K, in 1992 in electrical engineering. From 1989 to 1992, he was a Research Associate/Fellow in School of Electronic and Information Technology at Sheffield Hallam University. Between 1993 and 1999, he was a Senior Research Fellow, Principal Research Engineer, Associate Professor at Singapore Research Institute and Industry. In 2000, he joined the Singapore National Research Institute of High Performance Computing as a Principal Scientist (Full Professor) and Director of the Electronic and Photonics Department. He was the Guest Professor of Xi'an Jiaotong University and Peking University in China, External Academy Advisor to City University of Hong Kong, Global Advisory Board to KAIST, Korea. He authored or coauthored over 200 papers published in the referred international journals.

Dr. Li is a Fellow of IEEE, and a Fellow of Electromagnetics Academy, USA. He is the recipient of IEEE EMC Technical Achievement Award, Singapore IES Prestigious Engineering Achievement Award, and IEEE Sustained Service Award for EMC. He was the IEEE EMC Distinguished Lecturer from 2007 to 2008. He served as an Associate Editor for the IEEE Microwave and Wireless Components Letters from 2006 – 2008 and served Guest Editor for 2006 and 2010 IEEE Transactions on EMC Special

Issues, Guest Editor for 2010 IEEE Transactions on MTT APMC Special Issue. He is currently an Associate Editor for IEEE Transactions on CPMT and IEEE Transactions ON EMC. He is the Founding Member of IEEE MTT-RF Nanotechnology Committee. He has been a General Chair and Technical Chair for many international conferences. He was the President for 2006 International Zurich Symposium on EMC, the General Chair for the 2008 &2010 Asia-Pacific EMC Symposium, General Chair for 2010 IEEE Symposium on Electrical Design for Advanced Packaging Systems and the Chairman of the IEEE EMC Singapore Chapter for 2005 – 2006. He has been invited to give numerous invited talks and plenary speeches at various international conferences and forums.